Journal of Engineering Mathematics **43:** 385–399, 2002.

An analytical solution for mechanical etching of glass by powder blasting

J.H.M. TEN THIJE BOONKKAMP and J.K.M. JANSEN
Department of Mathematics and Computer Science, Eindhoven University of Technology, PO Box 513, 5600MB Eindhoven, The Netherlands

Received 24 April 2001; accepted in revised form 6 May 2002

Abstract. Masked erosion of glass by powder blasting is studied and a nonlinear partial differential equation of first order describing the displacement of the glass surface is proposed. This equation is solved by means of the characteristic-strip equations. If so-called transition regions are introduced near the edges of the mask, an analytical solution can be obtained which is in reasonable agreement with measurements.

Key words: characteristic-strip equations, powder blasting, shocks, single PDE of first order

1. Introduction

The increase in size of modern television screens has driven a trend towards lightweight, shallow displays to replace the current heavy, bulky cathode-ray-tube displays. Several basic principles for display design have been studied or are still being researched; for an overview see *e.g.* [1]. Some of these display principles require a vacuum enclosure for their operation; see *e.g.* [2]. In order to make lightweight displays, internal structures are required to support the vacuum envelope. Since these structures should not get in the way of the display function, they must be positioned very accurately. Furthermore, they should consist of dielectric material that has the same thermal expansion coefficient as the transparent, vacuum-proof front panel. Therefore, only structures of inorganic glass or ceramics are appropriate. In [2] a display is studied which makes use of thin, patterned glass plates as supporting structure, where electrons can travel through holes or trenches in the glass plates. These glass plates thus have to be very accurately patterned with holes or trenches over large surfaces (up to 1 m^2).

The high-accuracy patterning of glass plates at low cost is still an ongoing challenge. A promising technique studied here for this purpose is the mechanical etching by solid particle erosion, more commonly named powder- or sandblasting [3]. Patterned etching by sandblasting has been used mainly for the decoration of glass and mirrors, where the scattering of light at eroded parts of the surface contrasts attractively with the smooth unaffected parts of the surface. Although the decorative application has been used for many years, it did not need fundamental understanding. Furthermore, the erosion mechanism at the basis of the process, namely solid-particle impact, has been studied scientifically as the undesirable phenomenon damaging aircraft and rocket parts. Since this effort was primarily directed towards preventing erosion, little was known about the implications of using solid-particle erosion as a high-accuracy industrial etching process.

The physics of solid-particle erosion is presented in [4]. In particular, the erosion rate of an uncovered glass plate blasted with an abrasive powder is studied. Conversely, in this paper

we investigate the formation of patterns by erosion of surfaces that are locally protected with an erosion-resistant mask. We present a first model for the evolution of a substrate surface under the continuous impact of particles. The problem posed has some similarities with the erosion of structures at far finer scales, using ion-sputtering; see *e.g.* [5–8]. In this field models have been derived to describe the evolution of surfaces in 2D and 3D. The characteristics of the solid-particle erosion process, however, differ in a number of ways from that of ion-sputtering, posing specific problems and making the ion-sputtering experience of limited use for the powder-blasting process.

We have organized our paper as follows. In Section 2 we give a brief outline of the physics of powder erosion. In particular, we propose a model for the erosion rate E, based on measured data. Subsequently, in Section 3, we present a mathematical model for the erosion of glass, which consists of a hyperbolic partial differential equation for the surface position ζ or its slope p. In Section 4 we formulate the corresponding characteristic-strip equations, which that are solved in Section 5.

2. Physics of powder erosion

In powder erosion of brittle materials, sharp and abrasive particles in the powder cause deformations and micro-cracks in the target material. The formation of micro-cracks can be described by the kinetic energy of the erosive particles [4]. Chipping of target material above the cracks is the dominant erosion mechanism. The rate at which substrate material is removed is determined by the erosion rate E, which is defined as the ratio of the mass loss of the substrate and the mass of the erodent used.

There are several models for the erosion rate [4, 9–11]. In all these models, the erosion rate depends on the particle impact velocity $\mathbf{v}$. At normal impact, the erosion rate is proportional to a power of the magnitude of the impact velocity, *i.e.*

$$E = C\,|\mathbf{v}|^k, \tag{1}$$

where $C > 0$ is an empirical constant. Also, the exponent k is determined experimentally, and its value varies between 2 and 4 [12]. This is in agreement with theoretical models that predict the value $k = 7/3$; see *e.g.* [4, 9].

At oblique impact the erosion rate decreases. In this case, the erosion rate is roughly proportional to the component of the impact velocity normal to the substrate [13–16]. This can be observed from Figure 1, which shows the erosion rate of glass exposed to alumina (Al_2O_3) particles, as a function of the normal component of the impact velocity; see also [17, 18]. Therefore, we adopt the following model:

$$E = C\big(\,|\mathbf{v}|\cos\vartheta\big)^k, \tag{2}$$

where ϑ is the angle between the impact velocity vector $\mathbf{v}$ and the inward normal $\mathbf{n}$ to the surface and $C = C(\vartheta)$. Note that for $\vartheta = 75°$, *i.e.*, at glancing contact the factor C in (2) is somewhat different from the value at smaller angles ϑ. As C is weakly dependent on ϑ, it is henceforth assumed constant.

Figure 2 shows the formation of a pattern in a glass plate by masked erosion. The mask considered has a circular hole and is exposed to a constant particle mass flux, *i.e.*, the particle flux and the impact velocity are constant. The photographs have been made by time-lapse photography, exposing a picture at fixed time intervals. Some characteristics of the erosion

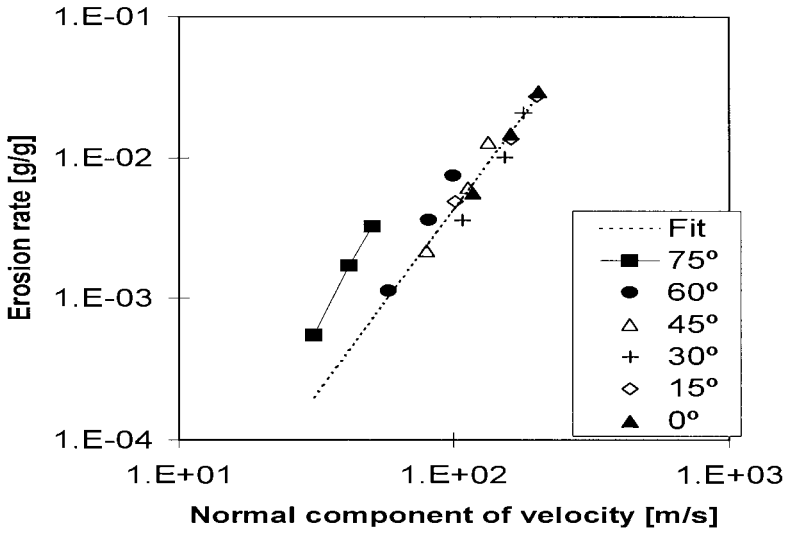

Figure 1. The erosion rate of glass as a function of the normal component of the impact velocity. The figures in the box give the angle between the impact velocity and the inward normal to the surface. (courtesy P.J. Slikkerveer, Philips Research Laboratories, Eindhoven)

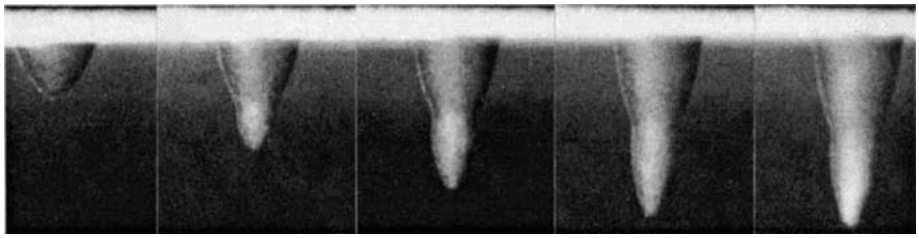

Figure 2. Pattern formation in glass by masked erosion. (courtesy P.J. Slikkerveer, Philips Research Laboratories, Eindhoven)

process can be seen from these photographs. First, the hole is shallow close to the edge of the mask and has a sharp tip in the middle. The reason for this is that, due to the finite particle size, not all particles contribute to the erosion process close to the mask. On the other hand, for a wide, shallow hole we would get a flat bottom in the centre. Secondly, with increasing depth, the rate of growth of the hole decreases. This can be explained by the dependence of the erosion rate on the angle of impact ϑ. Finally, with increasing depth, the hole takes an udder shape. This is probably caused by rebounding particles from the steep slopes at the sides of the pattern [7]. These particles are focused to the centre of the pattern, where they generate additional erosion. We will not consider this so-called second-strike effect in this paper.

3. Mathematical model for powder erosion

In this section we introduce a mathematical model for the displacement of a surface due to erosion by abrasive particles. Subsequently, we consider two special cases, *viz.* a two-dimensional trench and a rotationally symmetric hole.

Consider an initially flat substrate of brittle material, covered with a mask. In Figure 3 we introduce an (x, y, z)-coordinate system, where the (x, y)-plane coincides with the initial substrate and where the positive z-axis is directed into the material. A flux of particles with

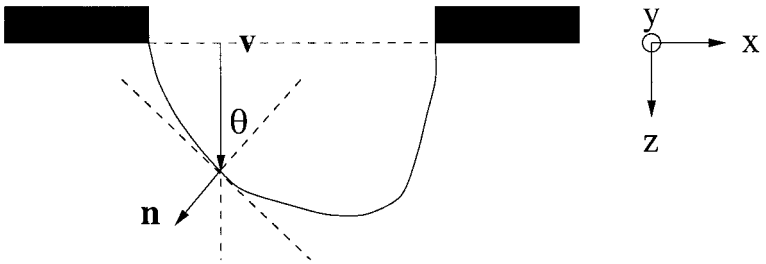

Figure 3. Cross section of a hole in the substrate.

velocity **v** in the positive z-direction hits the substrate and removes material. The position of the surface at time t is described by the function $z = \zeta(x, y, t)$. We now derive a kinematic condition for the surface. Let c denote the velocity of the surface in the direction of the unit normal **n** on the surface, which is directed into the material and is given by

$$\mathbf{n} = \frac{1}{\sqrt{1+\zeta_x^2+\zeta_y^2}} \begin{pmatrix} -\zeta_x \\ -\zeta_y \\ 1 \end{pmatrix}. \tag{3}$$

Consider a point $P(x_0, y_0, z_0)$ on the surface at time t_0. During a small time interval δt this point is displaced over a distance $c\,\delta t$ in the direction of **n** to the point $P'(x_0+\delta x, y_0+\delta y, z_0+\delta z)$. It is clear that the dispacements δx, δy and δz are given by

$$\begin{aligned} \delta x &= c\delta t \mathbf{n}\cdot\mathbf{e}_x = -\frac{c\delta t\zeta_x}{\sqrt{1+\zeta_x^2+\zeta_y^2}}, \\ \delta y &= c\delta t \mathbf{n}\cdot\mathbf{e}_y = -\frac{c\delta t\zeta_y}{\sqrt{1+\zeta_x^2+\zeta_y^2}}, \\ \delta z &= c\delta t \mathbf{n}\cdot\mathbf{e}_z = \frac{c\delta t}{\sqrt{1+\zeta_x^2+\zeta_y^2}}. \end{aligned} \tag{4}$$

On the other hand, we have

$$\begin{aligned} \delta z &= \zeta(x_0+\delta x, y_0+\delta y, t_0+\delta t) - \zeta(x_0, y_0, t_0) \\ &= \zeta_x(x_0, y_0, t_0)\delta x + \zeta_y(x_0, y_0, t_0)\delta y + \zeta_t(x_0, y_0, t_0)\delta t + \mathcal{O}(\delta t^2). \end{aligned} \tag{5}$$

Combining formulae (4) and (5) and taking the limit $\delta t \to 0$, we obtain the following equation for ζ:

$$\zeta_t - c\sqrt{1+\zeta_x^2+\zeta_y^2} = 0. \tag{6}$$

Initial and boundary conditions for (6) will be specified later.

For c we adopt the model [17]

$$c = \frac{1}{\rho_s} E\boldsymbol{\Phi}\cdot\mathbf{n} = \frac{1}{\rho_s} E\Phi\cos\vartheta, \tag{7}$$

where ρ_s is the mass density of the substrate, E the erosion rate, $\Phi = \Phi \mathbf{e_z}$ the particle mass flux in the direction of $\mathbf{v}$ and ϑ the angle between $\mathbf{v}$ and $\mathbf{n}$. This means that only the particle flux perpendicular to the surface contributes to the velocity c of the surface. Likewise, the erosion rate E only depends on the normal component $\mathbf{v} \cdot \mathbf{n}$ of the particle velocity $\mathbf{v} = v\mathbf{e}_z$, and is given by (2). Substitution of (7) and (2) in (6) gives

$$\zeta_t - \frac{C}{\rho_s} v^k \Phi \left(1 + \zeta_x^2 + \zeta_y^2\right)^{-k/2} = 0, \tag{8}$$

where we have used that $\cos \vartheta = 1/\sqrt{1 + \zeta_x^2 + \zeta_y^2}$.

Next, we make Equation (8) dimensionless. Introducing a characteristic length scale L, a characteristic particle mass flux $\tilde{\Phi}$ and the characteristic time $T = L\rho_s/(C\tilde{\Phi}v^k)$, we obtain in a straightforward way

$$\zeta_t - \Phi(x, y)\left(1 + \zeta_x^2 + \zeta_y^2\right)^{-k/2} = 0. \tag{9}$$

The characteristic length L can be the width of a two-dimensional trench or the radius of a rotationally symmetric hole. Note that T is the time needed to propagate the surface over a distance L, when the particles hit the surface perpendicularly with mass flux $\tilde{\Phi}$. In the derivation of (9) we have assumed that $v = \text{Const}$, which implies that the dimensionless particle mass flux $\Phi(x, y) = 1$. However, in the next section we will show that this choice for the particle mass flux does not give the correct solution of (9). A better model for the particle mass flux $\Phi(x, y)$ will be specified in Section 4.

As a first special case we consider the growth of a two-dimensional trench. Let x denote the transverse coordinate in the trench as indicated in Figure 3; then Equation (9) reduces to

$$\zeta_t + \Phi(x) f(\zeta_x) = 0, \quad 0 < x < 1, t > 0, \tag{10}$$

where the function $f = f(p)$ is defined by

$$f(p) = -\left(1 + p^2\right)^{-k/2}. \tag{11}$$

Equation (10) is supplemented with the following initial and boundary conditions:

$$\zeta(x, 0) = z_0(x), \quad 0 < x < 1, \tag{12}$$

$$\zeta(0, t) = \zeta(1, t) = 0, \quad t > 0. \tag{13}$$

For the initial profile $z_0(x)$ we usually take $z_0(x) = 0$; however, other choices are possible. The boundary conditions in (13) mean that the trench cannot grow at the ends $x = 0$ and $x = 1$. In Section 4 we will see that, for a suitable choice of the particle mass flux $\Phi(x)$, boundary conditions for ζ follow directly from the initial condition. For the special case $z_0(x) = 0$ we obtain (13); in this situation these boundary conditions are in fact redundant.

An alternative formulation of the formation of a trench is in terms of the slope $p = \zeta_x$. If we differentiate Equation (10) and initial condition (12) with respect to x, we obtain the following initial-value problem for p:

$$p_t + \left(\Phi(x) f(p)\right)_x = 0, \quad 0 < x < 1, t > 0, \tag{14}$$

$$p(x, 0) = z_0'(x), \quad 0 < x < 1. \tag{15}$$

Note that we do not have boundary conditions for p; however, we do not need these, as will become apparent in Section 4.

The second special case concerns the growth of a rotationally symmetric hole. Assume that the hole in the substrate has a circular shape. It is convenient to express Equation (9) in polar coordinates (r, ϕ), where the origin is located at the centre of the hole. Assuming rotational symmetry, we can write Equation (9) as

$$\zeta_t + \Phi(r) f(\zeta_r) = 0, \quad 0 < r < 1, t > 0. \tag{16}$$

Note that the particle mass flux now depends on r. Suitable initial and boundary conditions are

$$\zeta(r, 0) = z_0(r), \quad 0 < r < 1, \tag{17}$$

$$\zeta(1, t) = 0, \quad t > 0. \tag{18}$$

We have only one boundary condition at $r = 1$, stating that the hole does not grow at the edge. Also in this case, the boundary condition (18) is possibly redundant when $z_0(r) = 0$.

Both the two-dimensional trench and the rotationally symmetric hole are used in patterned glass plates. When the initial-boundary-value problems (10)–(13) and (16)–(18) are compared, it is clear that the profiles $\zeta = \zeta(x, t)$ for a two-dimensional trench and $\zeta = \zeta(r, t)$ for a cylindrically symmetric hole are alike. In the following, we only consider the two-dimensional trench problem.

4. Characteristic-strip equations

In this section we present the characteristic-strip equations of the initial-value problems (10)–(12) and (14)–(15). We assume that we have an initially flat substrate. Furthermore, we specify the particle mass flux Φ.

Consider the following partial differential equations for the surface position $\zeta(x, t)$ and its slope $p(x, t) = \zeta_x(x, t)$:

$$\begin{aligned} &\zeta_t - \Phi(x)\left(1 + \zeta_x^2\right)^{-k/2} = 0, \\ &p_t - \left(\Phi(x)\left(1 + p^2\right)^{-k/2}\right)_x = 0, \quad 0 < x < 1, t > 0, \end{aligned} \tag{19}$$

together with the initial conditions

$$\zeta(x, 0) = p(x, 0) = 0, \quad 0 < x < 1. \tag{20}$$

Introducing the variable $q = \zeta_t$, we can write the first partial differential equation in (19) in the canonical form

$$F(x, t, \zeta, p, q) := q - \Phi(x)\left(1 + p^2\right)^{-k/2} = 0. \tag{21}$$

The solution of the Cauchy problem for ζ, given by (21) and the corresponding initial condition in (20), can be constructed by solving the following initial-value problem [19]:

$$\begin{aligned}
\frac{\mathrm{d}x}{\mathrm{d}s} &= F_p = \Phi(x)\frac{kp}{(1+p^2)^{k/2+1}}, & x(0;\tau) &= \tau,\\
\frac{\mathrm{d}t}{\mathrm{d}s} &= F_q = 1, & t(0;\tau) &= 0,\\
\frac{\mathrm{d}\zeta}{\mathrm{d}s} &= pF_p + qF_q = \Phi(x)\frac{1+(k+1)p^2}{(1+p^2)^{k/2+1}}, & \zeta(0;\tau) &= 0,\\
\frac{\mathrm{d}p}{\mathrm{d}s} &= -(F_x + pF_\zeta) = \Phi'(x)\frac{1}{(1+p^2)^{k/2}}, & p(0;\tau) &= 0,\\
\frac{\mathrm{d}q}{\mathrm{d}s} &= -(F_t + qF_\zeta) = 0, & q(0;\tau) &= \Phi(\tau),
\end{aligned} \tag{22}$$

where s and τ are the parameters along the characteristics and the initial curve, respectively. The equations in (22) are referred to as the characteristic-strip equations. The initial condition for q follows from the partial differential equation (21) and the initial conditions for the other variables. At the same time, the first, second and fourth differential equation plus corresponding initial values determine the characteristics of the Cauchy problem for p, given by the second partial differential equations in (19) and the corresponding initial condition in (20). Note that the solution of the second and fifth equation is trivial, and we find

$$\begin{aligned}
t(s;\tau) &= s,\\
q(s;\tau) &= \Phi(\tau).
\end{aligned} \tag{23}$$

The formal solution procedure for the other equations is as follows. We solve the first, third and fourth equation and find $x = x(t;\tau)$, $\zeta = \zeta(t;\tau)$ and $p = p(t;\tau)$. Inverting the first function we have $\tau = \tau(x,t)$ and substitution of the latter expresssion gives the final solution $\zeta(x,t) := \zeta(t;\tau(x,t))$ and $p(x,t) := p(t;\tau(x,t))$. In the following we use the notation $v(t;\tau)$ or $v(x;\tau)$ for a generic variable v to indicate that an expression only holds along a characteristic parametrized by t or x. The parameter τ denotes that the characteristic passes through the point $(\tau,0)$. On the other hand, we use the notation $v(x,t)$ if an expression holds in a part of the (x,t)-plane.

A first obvious choice for the dimensionless particle mass flux would be $\Phi(x) = 1$. The solution of the initial-value problem (22) in this case is trivial, and we find $\zeta(x,t) = t$ and $p(x,t) = 0$, corresponding with a flat-bottom hole. This particular solution is in contrast with experimental results that show slanted sides near the edges of the mask; see Figure 2. As observed in Section 2, this is due to the finite particle size of the eroding powder which makes that not all particles are effective in the erosion process close to the mask. In order to model this phenomena, we introduce transition regions of thickness δ, where we assume that $\Phi(x)$ increases continuously and monotonically from 0 at the boundaries to 1 at $x = \delta, 1-\delta$. The parameter δ is characteristic of the (dimensionless) particle size and a typical value is $\delta = 0{\cdot}1$. We adopt the simplest possible choice for $\Phi(x)$, *i.e.*

$$\Phi(x) = \begin{cases} x/\delta & \text{if} \quad 0 \le x < \delta,\\ 1 & \text{if} \quad \delta \le x \le 1-\delta,\\ (1-x)/\delta & \text{if} \quad 1-\delta < x \le 1. \end{cases} \tag{24}$$

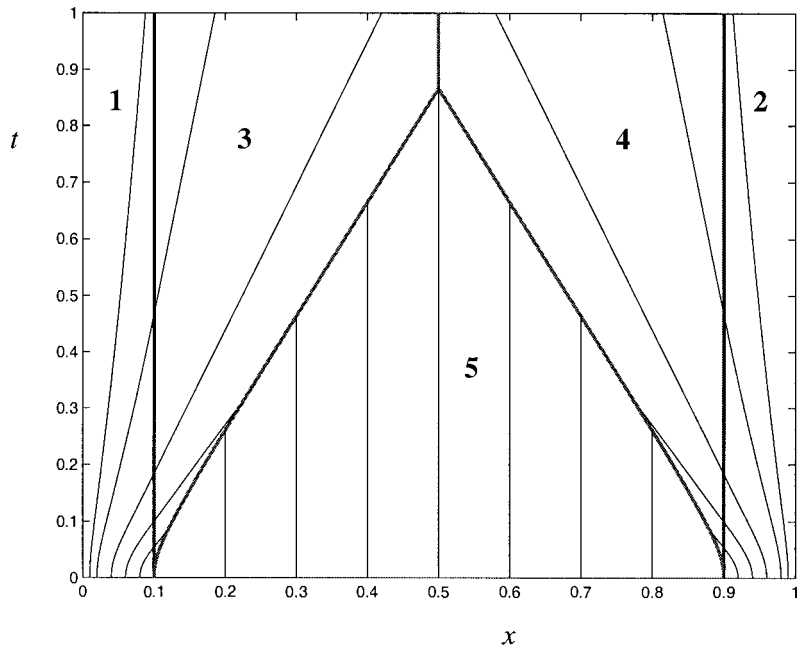

Figure 4. Characteristics and shocks of a two-dimensional trench, for $\delta = 0{\cdot}1$ and $k = 2$.

As a result of (24), the growth rate of the surface position close to the mask is smaller than in the middle of the hole. Since $\Phi(0) = \Phi(1) = 0$, we obtain from (22) the solutions $x(t;0) = \zeta(t;0) = 0$ and $x(t;1) = 1$, $\zeta(t;1) = 0$, implying that the boundary conditions (13) for ζ are automatically satisfied. Moreover, since $\Phi'(0) = 1/\delta$, we can compute $p(t;0)$ directly from the fourth equation in (22); likewise we can compute $p(t;1)$. Thus, we are not allowed to specify boundary conditions for p. However, the most important consequence of (24) is that charcteristics originating from the transition regions are directed into the interior domain for increasing t. This implies that the reduced particle mass flux in the transition regions will also influence the solution in the interior domain, which is in agreement with experimental results. Finally, we like to emphasize that (24) is merely a sensible guess for the particle mass flux that still allows computation of the analytical solution of (22). Other choices are possible.

By introducing transition regions, we create intersecting characteristics. Therefore, the solution of the partial differential equation for p in (19) can only be a weak solution [19] and it is anticipated that shocks will emerge from the edges $x = \delta$ and $x = 1 - \delta$. Let $x = \xi_{s,1}(t)$ and $x = \xi_{s,2}(t)$ denote the location of the shocks at time t originating at $x = \delta$ and $x = 1 - \delta$, respectively. Each point $(\xi_{s,i}(t), t)$ $(i = 1, 2)$ on these shocks is connected to two different characteristics that exist on both sides of the shocks. The speed of these shocks is given by the jump condition

$$\frac{\mathrm{d}\xi_{s,i}}{\mathrm{d}t}[p] = -[\Phi(x)(1 + p^2)^{-k/2}], \ (i = 1, 2), \tag{25}$$

where $[v]$ denotes the jump of a generic variable v across the shock. The derivation of (25) is based on the integral formulation of Equation (14) and is a standard result in the theory of first-order quasilinear partial differential equations; see *e.g.* [19]. Alternatively, in Appendix A we present a slightly different derivation, which is based on Equation (10). Thus, we can distinguish the following five regions in the (x, t)-plane: the left transition region $0 \leq x \leq \delta$

(region 1), the right transition region $1-\delta \leq x \leq 1$ (region 2), the interior domain left of the first shock (region 3), the interior domain right of the second shock (region 4) and the region between the two shocks (region 5); see Figure 4. Region 3 is the range of influence of the points in the left transition region, and likewise, region 4 is the range of influence of the points in the right transition region. In the following we will solve the system (22) in these five regions. Note, that the location of the shocks depends on the solution through the Equations (25) and has to be computed as well.

5. Analytical solution

The exact solution of the initial-value problem (22) is computed in this section. The special case $k = 2$ is discussed in [20].

First, consider region 1. If we choose x as the parameter along the characteristics instead of t, we can derive from (22) the following differential equations for the slope p and the surface position ζ,

$$\begin{aligned} \frac{\mathrm{d}p}{\mathrm{d}x} &= \frac{1}{x}\frac{1+p^2}{kp}, \\ \frac{\mathrm{d}\zeta}{\mathrm{d}x} &= \frac{1+(k+1)p^2}{kp}. \end{aligned} \tag{26}$$

Taking into account the initial conditions $x(0;\tau) = \tau$ and $p(0;\tau) = 0$ in (22), we can solve the first equation and find

$$p(x;\tau) = \sqrt{\left(\frac{x}{\tau}\right)^{2/k} - 1}. \tag{27}$$

Combining both differential equations in (26), we obtain the following simple equation for ζ

$$\frac{\mathrm{d}\zeta}{\mathrm{d}x} = p + \frac{1+p^2}{kp} = p + x\frac{\mathrm{d}p}{\mathrm{d}x}, \tag{28}$$

and together with the initial conditions $\zeta(0;\tau) = p(0;\tau) = 0$ in (22) it has the solution

$$\zeta(x;\tau) = xp(x;\tau). \tag{29}$$

The solutions in (27) and (29) give p and ζ along the characteristic through the point $(\tau, 0)$ on the initial curve. The location of this characteristic follows from the differential equation

$$\frac{\mathrm{d}x}{\mathrm{d}t} = \frac{k\tau}{\delta}\frac{\sqrt{(x/\tau)^{2/k} - 1}}{(x/\tau)^{2/k}}, \tag{30}$$

which follows readily after substitution of (27) in the differential equation for x in (22). Integrating (30) subject to the initial condition $x(0;\tau) = \tau$ and choosing p as the independent variable, we arrive at the relation

$$\frac{t}{\delta} = \mathcal{T}(p) := \int_0^p \left(1+r^2\right)^{k/2} \mathrm{d}r. \tag{31}$$

The integral in (31) can be expressed in terms of a hypergeometric function ${}_2F_1\big(a, b; c; z\big)$, resulting in the following alternative expression for t/δ [21, pp. 558]:

$$\frac{t}{\delta} = p\big(1+p^2\big)^{k/2}\,{}_2F_1\big(-k/2,\,1;\,3/2;\,\sin^2\vartheta\big), \quad \sin\vartheta = \frac{p}{\sqrt{1+p^2}}, \tag{32}$$

where ϑ is the angle between the impact velocity $\mathbf{v}$ and the inward normal $\mathbf{n}$; see Figure 3. Alternatively, formulae (31) and (32) can be obtained by direct integration of the differential equation for p in (22). Points (x,t) on the characteristic through $(\tau,0)$ are thus determined by (27) and (31). Note that the slope p in region 1 is a function of t/δ only and is independent of the space coordinate x. When computing the solution in region 1 at a given time level t, we first solve Equation (31) for p and subsequently compute ζ from (29).

From (27), (29) and (31), we see that the characteristic through $(\tau,0)$ $(0<\tau<\delta)$ reaches the edge $x=\delta$ at time $t_1(\tau)$, with slope $p_1(\tau)$ and surface position $\zeta_1(\tau)$ given by

$$\begin{aligned} p_1(\tau) &:= \sqrt{\left(\frac{\delta}{\tau}\right)^{2/k} - 1}, \\ \zeta_1(\tau) &:= \delta\, p_1(\tau), \\ t_1(\tau) &:= \delta\, \mathcal{T}(p_1(\tau)), \end{aligned} \tag{33}$$

with $\mathcal{T}(p)$ defined in (31). These are the 'initial' conditions for the solution of initial-value problem (22) in region 3.

Now, consider region 3. Since $\Phi'(x) = 0$ in region 3, the slope p is constant along characteristics and, consequently, the differential equations in (22) can be easily solved. We find

$$\begin{aligned} p(x;\tau) &= p_1(\tau), \\ \zeta(x;\tau) &= \zeta_1(\tau) + \frac{1+(k+1)p_1^2(\tau)}{kp_1(\tau)}(x-\delta), \\ t(x;\tau) &= t_1(\tau) + \frac{\big(1+p_1^2(\tau)\big)^{k/2+1}}{kp_1(\tau)}(x-\delta), \end{aligned} \tag{34}$$

with $p_1(\tau)$, $\zeta_1(\tau)$ and $t_1(\tau)$ defined in (33). The characteristics in this region are straight lines and are displayed in Figure 4. To compute the solution at a given point (x,t), we first have to solve the third equation in (34) for $p_1(\tau)$ and subsequently compute $p(x,t)$ and $\zeta(x,t)$ from the other two equations.

The solution of (22) in region 5 is trivial, and is given by

$$x(t;\tau) = \tau, \quad p(x,t) = 0, \quad \zeta(x,t) = t; \tag{35}$$

see Figure 4. The characteristics are now vertical lines through $(\tau,0)$, corresponding to a flat surface.

Since the particle mass flux (24) is symmetric around $x = 0{\cdot}5$, it is also clear that the solution of the initial-value problem (22) is symmetric around $x = 0{\cdot}5$. Consequently, the solution in regions 2 and 4 can be easily obtained from the corresponding solutions in region 1 and 3, respectively. However, for the sake of brevity, we omit the explicit formulae.

Finally, we have to determine the location of the shocks. We only consider the first shock, emanating from the edge $x=\delta$. The computation of the second shock is completely analogous. The evolution of the first shock is determined by the jump condition (25), which in this case leads to the initial-value problem

$$\frac{\mathrm{d}\xi_{s,1}}{\mathrm{d}t} = \frac{1}{p_{s,1}}\Big(1 - \big(1 + p_{s,1}^2\big)^{-k/2}\Big), \quad \xi_{s,1}(0) = \delta, \tag{36}$$

with $p_{s,1} = p_1(\tau)$ being the value of the slope just left of the shock on the characteristic through $(\delta, t_1(\tau))$. Thus, the following relation holds between $p_{s,1}$ and $\xi_{s,1}$:

$$\frac{\xi_{s,1} - \delta}{t - t_1(\tau)} = \frac{k p_{s,1}}{\big(1 + p_{s,1}^2\big)^{k/2+1}}. \tag{37}$$

Combining relation (37) with the formulae for $t_1(\tau)$ given in (33) and (31), differentiating the resulting equation with respect to t and substituting (36), we find the following initial-value problem for $p_{s,1}$:

$$\frac{\mathrm{d}p_{s,1}}{\mathrm{d}t} = \frac{p_{s,1}^2}{\big(1 + p_{s,1}^2\big)^{k/2}} \frac{\Big(k - \big(1 + p_{s,1}^2\big)\frac{\left(1+p_{s,1}^2\right)^{k/2}-1}{p_{s,1}^2}\Big)/\big(1 - p_{s,1}^2\big)}{\delta - \frac{(k+1)p_{s,1}^2-1}{p_{s,1}^2-1}\,\xi_{s,1}}, \quad p_{s,1}(0) = 0. \tag{38}$$

The initial value for $p_{s,1}$ follows, *e.g.* from Equation (31). Note that the right-hand sides of (36) and (38) are not defined for $t = 0$, and can only be computed using Taylor-series expansions for $\xi_{s,1}(t)$ and $p_{s,1}(t)$. The propagation of the shock is determined by the differential equations (36) and (38), which we have to solve numerically. The result is shown in Figure 4.

We have collected the results of this section in Figure 5, which gives the analytical solutions for ζ and p at time levels $t = 0{\cdot}0, 0{\cdot}1, \cdots, 1{\cdot}0$ for $\delta = 0{\cdot}1$ and $k = 2, 2{\cdot}33, 3, 4$. Figure 5 nicely displays the features of the solution: a slanted surface in the transition regions, a flat bottom in the interior domain and a curved surface in between. Also, the inwardly propagating shocks are clearly visible. Moreover, for increasing k, the slopes decrease, resulting in more shallow holes.

To validate our model, we compare in Figure 6 the analytical solution with experimental results at four different time levels, for the erosion of a trench. All surfaces are dimensionless according to the scaling in Section 3. We have computed the surfaces with $k = 7/3$ and $\delta = 0{\cdot}1$. We see a good qualitative agreement between analytical and experimental results. Both show the shallow, flat-bottom solution in the middle of the hole at $t = 0{\cdot}5$. However, the analytically computed hole at $t = 0{\cdot}5$ is somewhat deeper than the experimental one. The reason for this is probably the shadow effect of the mask, which is not included in the analytical model. For $t \geq 1{\cdot}6$, the experimental surfaces show an udder shape in the middle of the hole, which is probably caused by rebounding particles from the slopes at the sides of the surface. This so-called second-strike effect is also not included in our model. Further differences are the round top of the experimental holes, due to the finite particle size and the widening of the experimental holes due to mask wear.

6. Conclusion

Modern flat-screen televisions are equipped with a large glass plate with holes or trenches in it, to direct electrons to the proper spot on the screen. One method to manufacture such glass plates is to cover it with an erosion-resistant mask and blast it with an abrasive powder. In this paper we proposed a mathematical model for the formation of holes in a glass plate by powder-blasting. In particular, we derived a nonlinear partial differential equation of first order for the surface position ζ of a hole. We have computed an analytical solution for this equation

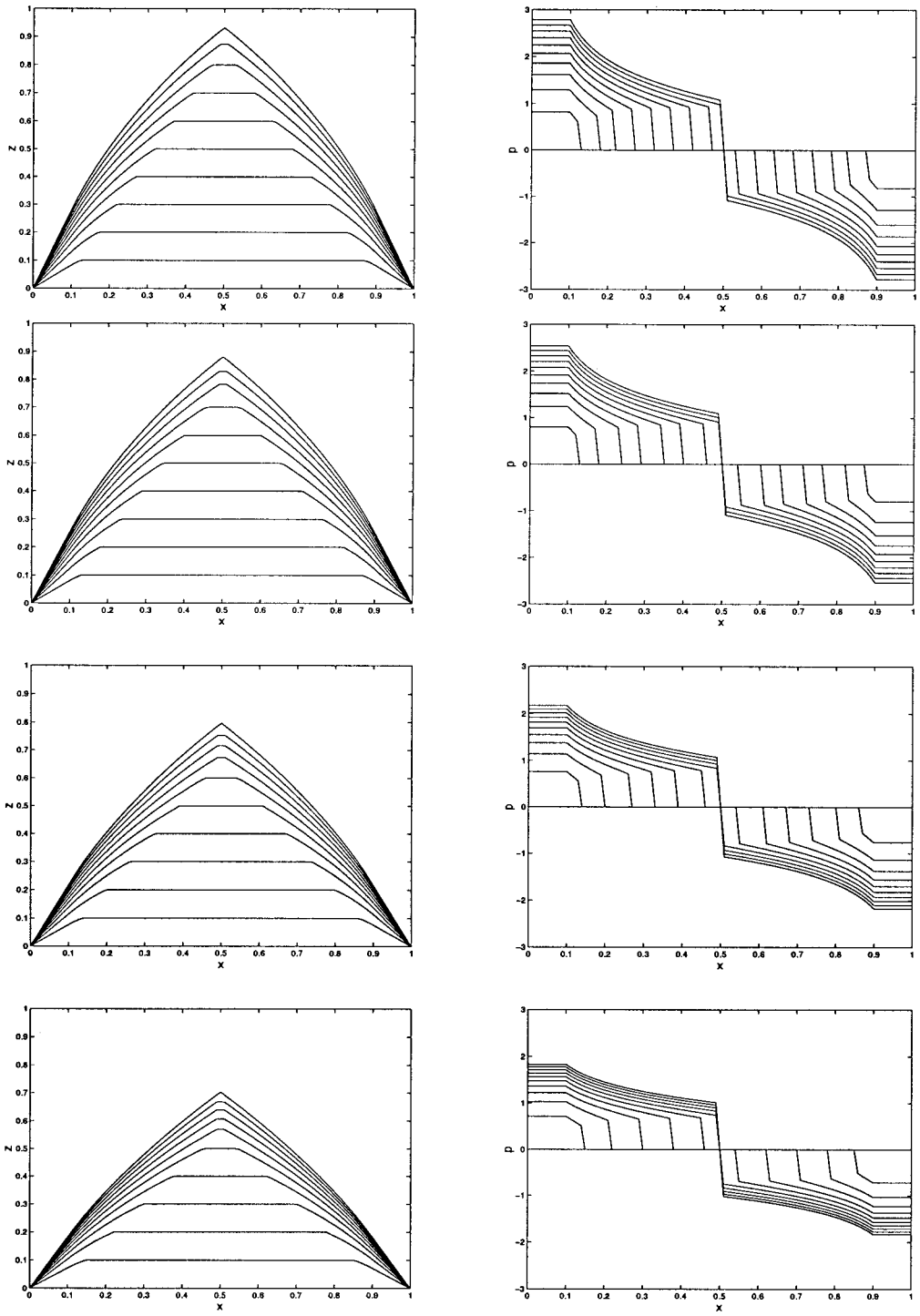

Figure 5. Analytical solution for the surface position (left) and its slope (right) of a two-dimensional trench. Parameter values are $\delta = 0{\cdot}1$ and (from top to bottom) $k = 2,\ 2{\cdot}33,\ 3$ and 4.

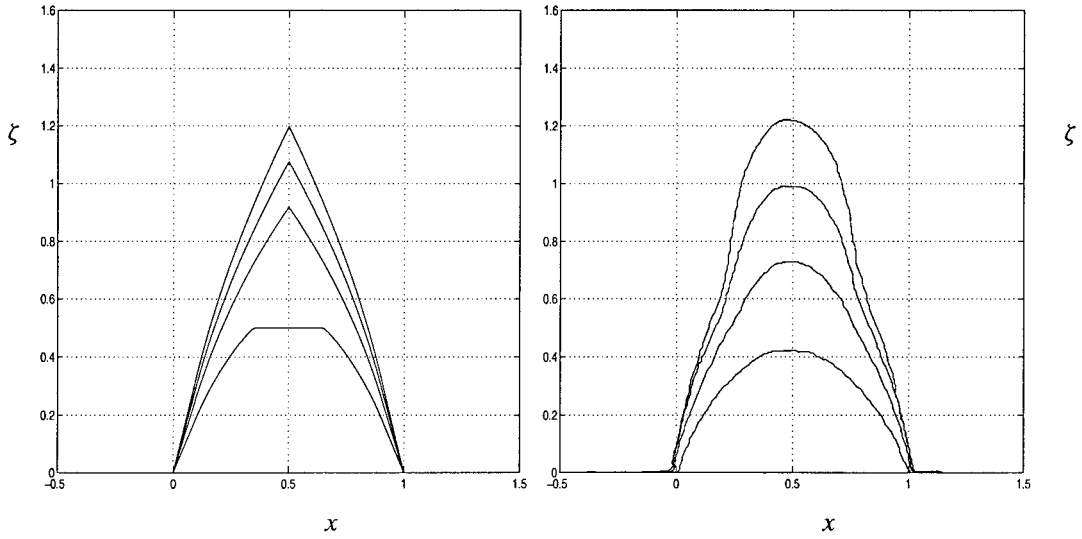

Figure 6. Analytical solution (left) and measurements (right) of the surface position for a two-dimensional trench at $t = 0{\cdot}5$, $1{\cdot}1$, $1{\cdot}6$ and $2{\cdot}1$. (Experimental results by P.J. Slikkerveer [20])

from the corresponding characteristic-strip equations and compared it with measurements. The analytical solution predicts a shallow hole with a slanted surface near the edges of the mask, connected with a deep, flat bottom in the middle of the hole. This is also observed in experiments. A discrepancy between the analytical solution and the experimental results is the formation of an udder-shaped surface in the middle of a hole. This is probably caused by rebounding particles and has not been taken into account in our model.

Topics for further research are, in our opinion, the modelling of rebounding particles, the so-called second-strike effect, and the application of level-set methods to this problem.

Appendix A, derivation of the jump condition

Equation (10) for the surface position $\zeta(x, t)$ can be written in the form

$$q + \Phi(x) f(p) = 0, \quad 0 < x < 1, t > 0, \tag{A.1}$$

with $p := \zeta_x$ and $q := \zeta_t$. This equation is a kinematic condition describing the displacement of the surface $z = \zeta(x, t)$ due to a normal velocity $c\mathbf{n}$; see Section 3. From Equation (A.1) we easily see that the relation

$$q(x_2, t) - q(x_1, t) + \Phi(x_2) f(p(x_2, t)) - \Phi(x_1) f(p(x_1, t)) = 0 \tag{A.2}$$

should hold for arbitrary $x_1, x_2 \in (0, 1)$, $t > 0$. We take $x_1 < x_2$. Assume that p and q, but not ζ, are discontinuous across a curve $\Gamma_s : x = \xi_s(t)$ in the domain $D : x_1 \leq x \leq x_2, t \geq 0$. The curve Γ_s divides D into two subdomains, *viz.* $D_1 : x_1 \leq x < \xi_s(t)$ and $D_2 : \xi_s(t) < x \leq x_2$, where we assume that ζ, p and q are continuously differentiable. We refer to Γ_s as a shock. Taking the limits $x_1 \uparrow \xi_s(t)$ and $x_2 \downarrow \xi_s(t)$, we obtain from (A.2)

$$[q] + \big[\Phi(x) f(p)\big] = 0, \tag{A.3}$$

with $[q] := q(\xi_s(t)+, t) - q(\xi_s(t)-, t)$ the jump in q across Γ_s; likewise $\big[\Phi(x) f(p)\big]$ is the jump in $\Phi(x) f(p)$ across Γ_s.

The difference $q(x_2, t) - q(x_1, t)$ in relation (A.2) can be split in three parts as follows:

$$q(x_2,t)-q(x_1,t) = \big(q(\xi_s(t)-,t)-q(x_1,t)\big)+\big(q(x_2,t)-q(\xi_s(t)+,t)\big) + \big(q(\xi_s(t)+,t)-q(\xi_s(t)-,t)\big) \tag{A.4a}$$

$$= \int_{x_1}^{\xi_s(t)} p_t(x,t)\,\mathrm{d}x + \int_{\xi_s(t)}^{x_2} p_t(x,t)\,\mathrm{d}x + [q]. \tag{A.4b}$$

The first and second term on the right-hand side of (A.4a) are the increments of $q(x,t)$ in D_1 and D_2, respectively, and they can be expressed by the integrals in (A.4b). The last term on the right-hand side of (A.4a) is just the jump of q across Γ_s. The integrals in (A.4b) satisfy the relations

$$\int_{x_1}^{\xi_s(t)} p_t(x,t)\,\mathrm{d}x = I_1'(t) - p(\xi_s(t)-,t)\xi_s'(t), \tag{A.5a}$$

$$\int_{\xi_s(t)}^{x_2} p_t(x,t)\,\mathrm{d}x = I_2'(t) + p(\xi_s(t)+,t)\xi_s'(t), \tag{A.5b}$$

where the integrals $I_1(t)$ and $I_2(t)$ are defined by

$$I_1(t) := \int_{x_1}^{\xi_s(t)} p(x,t)\,\mathrm{d}x = \zeta(\xi_s(t),t)-\zeta(x_1,t), \tag{A.6a}$$

$$I_2(t) := \int_{\xi_s(t)}^{x_2} p(x,t)\,\mathrm{d}x = \zeta(x_2,t)-\zeta(\xi_s(t),t). \tag{A.6b}$$

Inserting relations (A.5) into (A.4b), we obtain

$$q(x_2,t)-q(x_1,t) = I_1'(t)+I_2'(t)+[p]\,\xi_s'(t)+[q]. \tag{A.7}$$

Taking into account that $\zeta(x,t)$ is continuous at $x=\xi_s(t)$, we see that $I_1'(t)+I_2'(t) = q(x_2,t)-q(x_1,t)$ and consequently relation (A.7) reduces to

$$[p]\,\xi_s'(t)+[q]=0. \tag{A.8}$$

Combining (A.3) and (A.4b) we obtain the jump condition

$$[p]\,\xi_s'(t) = \big[\Phi(x)f(p)\big]. \tag{A.9}$$

Finally, substituting expression (11) for the function $f(p)$, we recover the jump condition (25).

Acknowledgements

The authors would like to thank J. Boersma for critically reading the manuscript and for many valuable suggestions which helped to improve the text.

References

1. L.E. Tannas Jr, *Flat Panel Displays and CRT's*. New York: Van Nostrand Reinhold (1985).

2. G.G.P. van Gorkom, T.S. Baller, B.H.W. Hendriks, N. Lambert, H.J. Ligthart, E.A. Montie, G.E. Thomas, P.H.F. Trompenaars and S.T. de Zwart, Flat thin CRT based on controlled electron transport through insulated surfaces. *Appl. Surf. Sci.* 111 (1979) 276–284.
3. H.J. Ligthart, P.J. Slikkerveer, F.H. in 't Veld, P.H.W. Swinkels and M.H. Zonneveld, Glass and glass machining in Zeus panels. *Philips J. Res.* 50 (1996) 475–499.
4. P.J. Slikkerveer, P.C.P. Bouten, F.H. in 't Veld and H. Scholten, Erosion and damage by sharp particles. *Wear* 217 (1998) 237–250.
5. G. Carter and M.J. Nobes, The theory of development of surface morphology by sputter erosion processes. In: O. Aucello and R. Kelly (eds), *Ion Bombardment Modification of Surfaces*. Amsterdam: Elsevier (1984) pp. 163–224.
6. I.V. Katardjiev, G. Carter, M.J. Nobes, S. Berg and H.O. Blom, Three dimensional simulation of surface evolution and erosion. *J. Vac. Sci. Technol.* A 12 (1994) 61–68.
7. R. Smith and J.M. Walls, The development of a general three-dimensional surface under ion bombardment. *Phil. Mag.* A 42 (1980) 235–248.
8. R. Smith, G. Carter and M.J. Nobes, The theory of surface erosion by ion bombardment. *Proc. R. Soc. London* A407 (1986) 405–433.
9. M. Buijs, Erosion of glass modelled by indentation theory. *J. Am. Ceram. Soc.* 77 (1994) 1676–1678.
10. L. Murugesh and R.O. Scattergood, Effect of erodent properties on the erosion of alumina. *J. Mater. Sci*. 26 (1991) 5456–5466.
11. I.M. Hutchings, Transitions, threshold effects and erosion maps. *Key Eng. Mater.* 71 (1992) 75–92.
12. Z. Feng and A. Ball, The erosion of four materials using seven erodents-towards an understanding. *Wear* 233-235 (1999) 674–684.
13. Y. Ballout, J.A. Mathis and J.E. Talia, Solid particle erosion mechanisms in glass. *Wear* 196 (1996) 263–269.
14. A.J. Sparks and I.M. Hutchings, Transitions in erosive wear of a glass ceramic. *Wear* 149 (1991) 99–110.
15. G.L. Sheldon, Similarities and differences in the erosion behaviour of materials. *Trans. ASME J. Basic. Eng.* 92 (1970) 619–626.
16. S.M. Wiederhorn, B.R. Lawn and B.J. Hockey, Effect of particle impact angle on strength degradation of glass. *J. Am. Ceram. Soc.* 62 (1979) 639–640.
17. P.J. Slikkerveer and F.H. in 't Veld, Model for patterned erosion. *Wear* 233-235 (1999) 377–386.
18. P.J. Slikkerveer, *Mechanical Etching of Glass by Powder Blasting*. Ph.D. Thesis, Eindhoven University of Technology (1999).
19. J. Kevorkian, *Partial Differential Equations, Analytical Solution Techniques*. Pacific Grove: Wadsworth & Brooks (1990) 547 pp.
20. J.H.M. ten Thije Boonkkamp and P.J. Slikkerveer, Mathematical modelling of erosion by powder blasting. *Surv. on Math. Ind.* 10 (2002) 89–105.
21. M. Abramowitz and I.A. Stegun (eds), *Handbook of Mathematical Functions*. Washington: National Bureau of Standards (1964) 1046 pp.